



New complexes of Cu(II) with dipicolinate and pyridyl-based ligands: An experimental and DFT approach



Florencia Luzardo^a, Natalia Álvarez^a, Carlos Kremer^a, Andrea S.S. de Camargo^b, Jorge S. Gancheff^{a,*}

^a Cátedra de Química Inorgánica, Departamento "Estrella Campos", Facultad de Química, CC 1157, 11800, Montevideo, Uruguay

^b São Carlos Physics Institute, University of São Paulo, São Carlos, Brazil

ARTICLE INFO

Article history:

Received 23 December 2016

Received in revised form 3 April 2017

Accepted 5 April 2017

Available online 08 April 2017

Keywords:

Coordination chemistry

Cu(II) complexes

Pyridyl-based ligands

DFT

TD-DFT

ABSTRACT

The three novel mononuclear copper(II) complexes with dipicolinate and pyridyl-based ligands [Cu(dipic)(L)(OH₂)] (L = 4-picoline, vinylpyridine, 4-styrylpyridine; dipic²⁻ = dipicolinate) were afforded and structurally characterized. X-ray diffraction studies accounted for slight distorted square-pyramidal structures in which the dianion dipic²⁻ acts as a tridentate ligand in a *mer*-fashion, the *N*-donor species occupy an in-plane position, and a water molecule was detected apically coordinated. To assess the effect of the nature of the pyridyl-substituent (*para* position) on electronic properties, other complexes were also synthesized: [Cu(dipic)(py)(OH₂)], [Cu(dipic)(OH₂)₂(μ-pyz)] and [Cu(dipic)(OH₂)(μ-pypy){Cu(dipic)}] (py = pyridine, pyz = pyrazine, pypy = (*E*)-1,2-bis(pyridine-4-yl)ethane). Absorptive behavior in the UV–VIS region was studied in solution and in the solid state (reflectance measurements).

Additionally, geometry and population analyses were conducted by means of DFT calculations. Electronic UV–VIS spectra were simulated for both dinuclear complexes in the framework of the TD-DFT methodology to assign the origin of the absorption bands.

© 2017 Elsevier B.V. All rights reserved.

1. Introduction

Pyridine-2,6-dicarboxylic acid (also known as dipicolinic acid, H₂dipic) represents a water-soluble, commercially available, low-cost and versatile *N,O,O*-chelating ligand, which exhibits multiple coordination modes acting as dianion (dipic²⁻), monoanion (Hdipic⁻), or in a neutral form (H₂dipic) [1–6]. Metal complexes containing these ligands have been successfully employed in the field of material chemistry [7–19], in medicine [20–28], and biology [29–35]. As a result of the versatility of dipicolinate, the number of X-ray crystal data of dipic-containing complexes is rather high, and those with Cu(II) in particular are not an exception. Despite this copious information, the synthesis of new Cu(II)-containing dipicolinate complexes still represents an open field of research.

Hence, in the context of the aforementioned considerations and as part of our interest on contributing to increment basic knowledge on chemical and physical properties of copper(II) complexes containing dipic and *N*-donor ligands, the synthesis, crystal structure and study of the absorptive behavior in solution and in the solid state (reflectance measurements) of the three novel mononuclear Cu(II) complexes [Cu(dipic)(L)(OH₂)] (L = 4-picoline, vinylpyridine, 4-styrylpyridine; dipic²⁻ = dipicolinate) is presented. In order to assess the role of the

N-donor ligand on the chemical properties and absorptive features, other complexes were also included: [Cu(dipic)(py)(OH₂)], [Cu(dipic)(OH₂)₂(μ-pyz)] and [Cu(dipic)(OH₂)(μ-pypy){Cu(dipic)}] (py = pyridine, pyz = pyrazine, and pypy = (*E*)-1,2-bis(pyridine-4-yl)ethane). Geometry optimization and population analysis (NPA) were conducted by B3LYP in combination with 6-31G(d) for the further understanding of geometric and electronic properties of all complexes. Electronic UV–VIS spectra were calculated in the TD-DFT framework in the gas phase and in the presence of the solvent to assign the origin of the absorption bands experimentally detected.

2. Experimental

2.1. General Procedures and Syntheses

All reagents and solvents were purchased from commercial sources, the last ones being purified and dried by common methods [36]. Elemental analyses for carbon, hydrogen and nitrogen were performed on a Carlo Erba EA1108 analyzer. IR spectra were recorded for the complexes dispersed in KBr pellets on a BOMEM MB 102 FT-IR spectrometer. UV–VIS spectra in solution were measured on a Shimadzu UV-1603 spectrophotometer, while those in the solid state (reflectance studies) were recorded on a Shimadzu UV-2600 spectrophotometer equipped with an integrating sphere model ISR-2600Plus.

* Corresponding author.

E-mail address: jorge@fq.edu.uy (J.S. Gancheff).

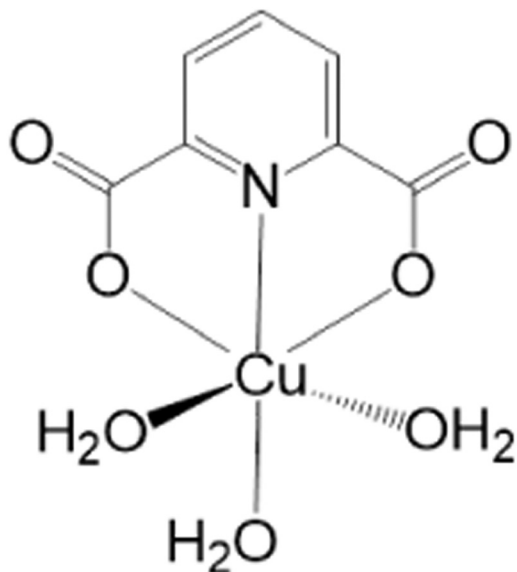
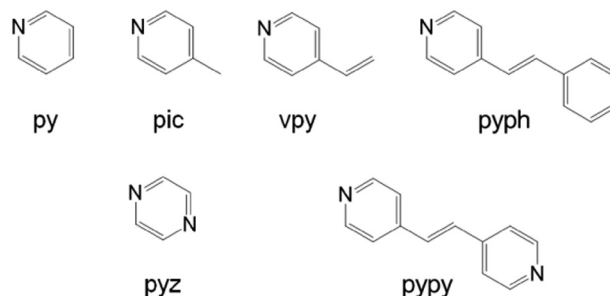
Table 1
Crystal, X-ray diffraction collection and structure refinement data.

Complex	3·2H ₂ O	4·2H ₂ O	5·H ₂ O
Chemical formula	C ₂₆ H ₃₂ Cu ₂ N ₄ O ₁₄	C ₁₄ H ₁₆ CuN ₂ O ₇	C ₄₀ H ₃₄ Cu ₂ N ₄ O ₁₁
Molecular weight	751.66	387.83	873.79
Crystal size (mm ³)	0.210 × 0.080 × 0.020	0.316 × 0.107 × 0.052	0.033 × 0.024 × 0.021
T (K)	293(2)	100(2)	293(2)
Crystal system	Triclinic	Triclinic	Monoclinic
Space group	P-1	P-1	P2 _{1/n}
Cell dimensions (Å, °)			
A	7.1863(5)	4.9845(3)	5.3379(3)
B	10.2688(7)	12.0021(10)	46.652(3)
C	10.8242(7)	13.0766(11)	7.8410(4)
α	97.878(2)	83.971(5)	90°
β	99.742(2)	87.848(4)	107.474(2)°
γ	102.079(2)	88.400(4)	90°
Volume (Å ³)	757.39(9)	777.20(10)	1862.48(17)
Z	1	2	2
ρ _{calc} (Mg m ⁻³)	1.648	1.657	1.558
θ _{min} , θ _{max} (°)	2.96, 26.45	3.135, 26.731	5.992, 74.761
Reflections collected	15,774	21,383	19,501
T _{min} , T _{max}	0.592, 0.745	0.6250, 0.7538	0.75, 0.96
Goodness-of-fit on F ²	1.098	1.002	1.169
Parameters, data	233, 3095	235, 3307	262, 3545
R ₁ , wR ₂ [I > 2σ(I)]	0.0322, 0.0745	0.0522, 0.0908	0.0608, 0.1606
R ₁ , wR ₂ [all data]	0.0458, 0.0803	0.1002, 0.1065	0.0689, 0.1648
Largest diff. peak, hole (e Å ⁻³)	0.325, -0.556	0.910, -0.646	0.532, -0.416

The ligands 4-styrylpyridine (pyph) and (*E*)-1,2-bis(pyridine-4-yl)ethene (pypy) were prepared by Knoevenagel condensation [37,38] under reaction conditions analogous to the ones made available by Bhomwik et al. [39]. The precursor *mer*-[Cu(dipic)(OH₂)₃] (**1**) was synthesized following a reported procedure [40]. Its purity was checked by elemental analyses and FT-IR measurements.

2.1.1. Synthesis of [Cu(dipic)(OH₂)(py)]·2H₂O (**2**·2H₂O)

A solution of 99 μL (0.125 mmol) of pyridine in MeOH (6 mL) was carefully layered on top of an aqueous solution (8 mL) of precursor **1** (35 mg, 0.125 mmol). Blue crystals of **2** were afforded after seven days (19 mg, 47%). Anal. calcd for CuC₁₂H₁₄N₂O₇: C, 39.84; N, 7.74; H, 3.34. Found: C, 39.92; N, 7.78; H, 3.38. IR (KBr) ν_{max}: 3432 (O–H_w), 3100–3065 (Csp²–H), 1639 (COO), 1429 cm⁻¹ (Ar). UV–VIS (MeOH) λ_{max},

**Scheme 1.** View of the precursor [Cu(dipic)(OH₂)₃].**Fig. 1.** View of the pyridyl-based ligands employed in this work: pyridine (py), 4-picoline (pic), vinylpyridine (vpy), 4-styrylpyridine (pyph), pyrazine (pyz), and (*E*)-1,2-bis(pyridine-4-yl)ethene (pypy).

nm: 223 (sh), 244, 249, 256, 262, 270, 277, 724; UV–VIS (solid state) λ_{max}, nm: 220 (sh), 247, 275 (sh), 385 (sh), 720.

2.1.2. Synthesis of [Cu(dipic)(OH₂)(pic)]·2H₂O (**3**·2H₂O)

A solution of 120 μL (0.125 mmol) of 4-picoline in MeOH (6 mL) was carefully layered on top of an aqueous solution (8 mL) of precursor **1** (35 mg, 0.125 mmol). Blue crystals of **3**, suitable for X-ray diffraction studies, were obtained after three days (19 mg, 43%). Anal. calcd for CuC₁₃H₁₆N₂O₇: C, 41.54; N, 7.45; H, 4.29. Found: C, 41.64; N, 7.66; H, 4.29. All values are given as percentages. IR (KBr) ν_{max}: 3420 (H₂O), 3080–3040 (Csp²–H), 1623 (COO), 1429 cm⁻¹ (Ar). UV–VIS (MeOH) λ_{max}, nm: 222, 254, 260, 267, 276, 757; UV–VIS (solid state) λ_{max}, nm: 220, 248, 273, 396 (sh), 710.

2.1.3. Synthesis of [Cu(dipic)(OH₂)(vpy)]·2H₂O (**4**·2H₂O)

A methanolic solution (6 mL) containing 133 μL (0.125 mmol) of vpy was layered on top of **1** (35 mg, 0.125 mmol) in 8 mL of H₂O. Blue crystals of **4** – suitable for X-ray diffraction measurements – were yielded after five days (26 mg, 46%). Anal. calcd for CuC₁₄H₁₆N₂O₇: C, 43.36; N, 7.22; H, 4.16. Found: C, 43.78; N, 7.88; H, 4.63 (all values are given in percentages). IR (KBr) ν_{max}: 3428 (H₂O), 3065–3035 (Csp²–H), 1645 (COO), 1430 (Ar). UV–VIS (MeOH) λ_{max}, nm: 251, 260 (sh), 268, 270 (sh), 277 (sh), 746; UV–VIS (solid state) λ_{max}, nm: 222, 252, 292, 429, 682.

2.1.4. Synthesis of [Cu(dipic)(OH₂)(pyph)]·H₂O (**5**·H₂O)

A methanolic solution (6 mL) containing 22.6 mg (0.125 mmol) of pyph was layered on top of **1** (35 mg, 0.125 mmol) in 8 mL of H₂O. Blue crystals of **5**, suitable for X-ray diffraction measurements, were yielded after five days (24.6 mg, 46%). Anal. calcd for CuC₂₀H₂₀N₂O₇: C, 51.78; N, 6.04; H, 4.34. Found: C, 51.81; N, 5.99; H, 4.27 (all values

Table 2
Selected bond lengths (Å) and bond angles (°) for complexes **3**·2H₂O, **4**·2H₂O and **5**·H₂O.

Complex	Bond lengths (Å)			
	3·2H ₂ O	4·2H ₂ O	5·H ₂ O	
Cu–O1	2.2376(23)	2.2120(25)	2.3914(33)	
Cu–O2	2.0392(15)	2.0544(25)	1.9987(35)	
Cu–O3	2.0566(14)	2.0337(25)	2.0459(30)	
Cu–N1	1.9122(21)	1.9056(39)	1.8991(34)	
Cu–N2	1.9566(19)	1.9547(38)	1.9522(39)	
Complex	Bond angles (°)			
	3·2H ₂ O	4·2H ₂ O	5·H ₂ O	
	O1–Cu–O2	91.127(69)	90.948(96)	92.465(126)
	O1–Cu–O3	94.718(69)	97.825(96)	88.079(123)
	O2–Cu–O3	159.467(65)	159.308(103)	161.568(126)
	O1–Cu–N1	94.654(85)	96.798(124)	90.309(125)
	O1–Cu–N2	97.132(81)	94.902(121)	95.913(136)
	N1–Cu–N2	168.211(82)	168.164(160)	173.731(146)

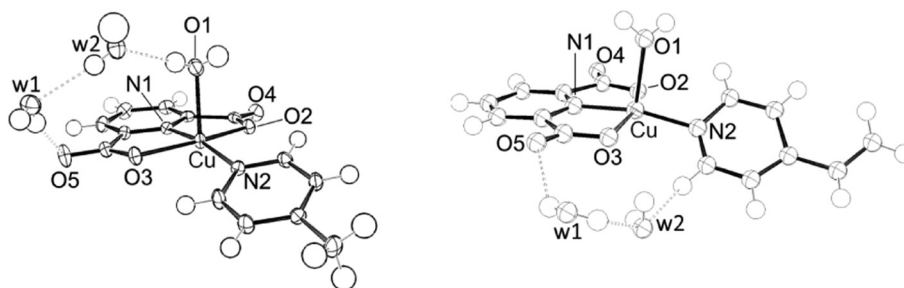


Fig. 2. Molecular structure and labelling for **3**·2H₂O (left), and **4**·H₂O (right) (H-bonds are displayed by dashed lines). Thermal ellipsoids are drawn at the 30% probability level.

are given in percentages). IR (KBr) ν_{\max} : 3392 (H₂O), 3071 (Csp²-H), 1648 (COO), 1434 cm⁻¹ (Ar). UV-VIS (MeOH) λ_{\max} , nm: 224, 235 (sh), 268 (sh), 278 (sh), 296 (sh), 306, 325 (sh), 735; UV-VIS (solid state) λ_{\max} , nm: 223, 264, 340, 675.

2.1.5. Synthesis of $[\{Cu(dipic)(OH_2)\}_2(\mu-pyz)]$ (**6**)

Crystals of this complex were afforded according to the technique of Felloni et al. [40]. IR (KBr) ν_{\max} : 3392 (H₂O), 3071 (Csp²-H), 1627 (COO), 1434 (Ar). UV-VIS (MeOH) λ_{\max} , nm: 224 (sh), 253 (sh), 260, 267, 277 (sh), 313 (sh), 720; UV-VIS (solid state) λ_{\max} , nm: 220 (sh), 260, 365 (sh), 672.

2.1.6. Synthesis of $[\{Cu(dipic)(OH_2)\}(\mu-pypy)\{Cu(dipic)\}]$ (**7**)

This complex was obtained by employing a reported protocol [40]. The low solubility of this compound in common solvents obstructed the characterization in solution. IR (KBr) ν_{\max} : 3392 (H₂O), 3010 (Csp²-H), 1642 (COO), 1424 (Ar). UV-VIS (solid state) λ_{\max} , nm: 220 (sh), 272, 291, 318 (sh), 340, 675.

2.2. X-ray Diffraction Studies

Data for suitable single crystals were collected with a Bruker D8 Venture diffractometer equipped with a Photon 100 CMOS detector using a curved-graphite-monochromated Mo-K α radiation ($\lambda = 0.71073$ Å). The data collection and data reduction were performed with the APEX2 [41] set of programs. Multi-scan absorption correction was applied [42]. The solutions of structures were found with the SHELXT package, and were refined with SHELXL-2014 [43] within SHELXL [44]. All non-hydrogen atoms were refined using anisotropic displacement parameters. Carbon-bonded hydrogen atoms were stereochemically positioned, and isotropically refined using the riding-model. Thermal parameters were set at 1.2 times the U_{eq} of the carbon atom they are bonded to. Water-hydrogen atoms were found in the difference Fourier map; they were positionally fixed, and their thermal parameters were set to 1.5 times the U_{eq} of the oxygen atom. ORTEP-3 for Windows [45] was used for drawings. Summary of the crystallographic data, experimental details and refinement results are listed in Table 1.

2.3. Theoretical Calculations

All calculations were undertaken at the density functional theory (DFT) level of theory. Geometry optimizations starting from molecular structures determined by X-ray crystallography were conducted [40, 46,47]. In all cases, B3LYP [48] in combination with 6-31G(d) [49] was employed, and an ultrafine grid featured by 90 radial shells and 590 angular points per shell was taken into account. The nature of the stationary point was verified through vibrational analysis (no imaginary frequencies at the minimum).

The Time-Dependent DFT (TD-DFT) methodology was employed to calculate up to four hundred spin-allowed transitions in the gas phase, and in the presence of the solvent by employing B3LYP/6-31G(d) for di-copper complexes. All effects of solvent were described by the conductor-like polarizable continuum model (C-PCM) [50], which is a valid model to consider the effects of the solvent as long as the specific interaction between the solute and the solvent are not of a significant importance. Electronic UV-VIS spectra were simulated by means of the GaussSum software [51] considering all calculated excitations. Natural Population Analysis (NPA) calculations were performed with the NBO code [52] included in the program package Gaussian 09, Rev. D01 [53], which was used for all theoretical studies reported in this contribution.

3. Results and Discussion

3.1. Synthesis and Crystal Structure

All complexes of Cu(II) were afforded by a simple substitution reaction starting from the precursor *mer*-[Cu(dipic)(OH₂)₃] (Scheme 1). The strategy of layering an alcoholic solution of the *N*-donor ligand (see Fig. 1) on an aqueous solution of the precursor resulted simple, reproducible and led to the desired complex in reasonable yield.

Selected interatomic distances and bond angles are summed up in Table 2. Metric data are typical of square-pyramidal geometries (Figs. 2 and 3). An oxygen atom (O1) from a water molecule is detected apically coordinated. Distances Cu—O1 resulted of 2.2376 Å (**3**·2H₂O), 2.2120 Å (**4**·2H₂O), and 2.3914 Å (**5**·H₂O), the last one being located more remote due to a H-bond O1⋯H(w1) with distance of

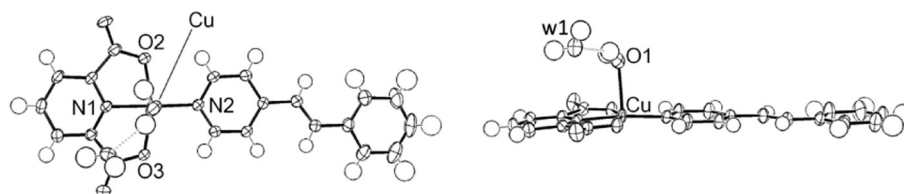


Fig. 3. Molecular structure (up-view, left; front-view, right) and labelling for complex **5**·H₂O (H-bond is displayed by dashed lines). Thermal ellipsoids are drawn at the 30% probability level.

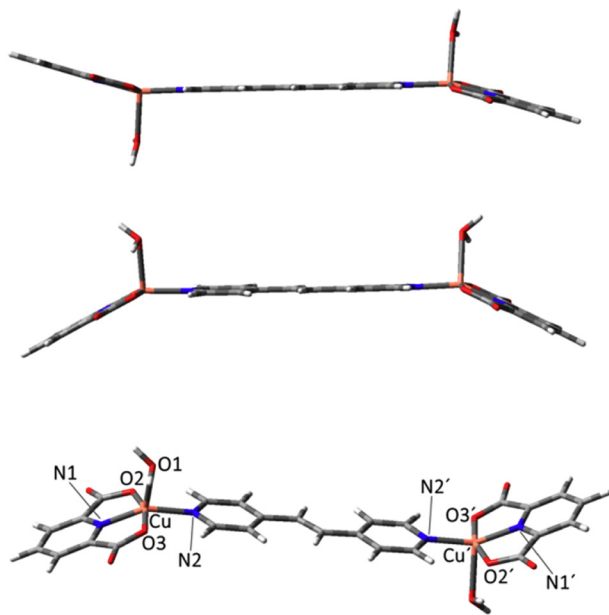


Fig. 4. Front-view of the optimized geometry of *trans*-7 (top), and of *cis*-7 (medium) as calculated in the gas phase with B3LYP/6-31G(d) ($T = 298$ K). Atom labelling is also included (bottom).

1.8888(62) Å (Fig. 3). Three of the in-plane coordination sites are occupied by the dipic fragment, which keeps the *mer*-orientation observed in the precursor. Distances for Cu—N1 (dipic) are of 1.9122 Å ($3 \cdot 2\text{H}_2\text{O}$), 1.9056 Å ($4 \cdot 2\text{H}_2\text{O}$), and 1.8991 Å ($5 \cdot \text{H}_2\text{O}$), while the basal fourth position is occupied by the nitrogen atom of the pyridyl-based ligand with distances (in Å) of 1.9566, 1.9547, and 1.9522 for $3 \cdot 2\text{H}_2\text{O}$, $4 \cdot 2\text{H}_2\text{O}$, and $5 \cdot \text{H}_2\text{O}$, respectively. These results are in accordance with the ones reported by Felloni et al. [40] H-bonds were also detected in

Table 3
Selected optimized parameters (bond lengths in Å, bond angles in °) for complexes 2–7 as obtained with B3LYP/6-31G(d) in the gas phase ($T = 298$ K).

Bond lengths						
Complex	2	3	4	5	6	7 ^a
Cu—O1	2.324	2.331	2.332	2.333	2.277	2.321 (2.322)
Cu—O2	1.952	1.953	1.953	1.954	1.997	1.951 (1.951)
Cu—O3	2.018	2.021	2.021	2.022	1.942	2.016 (2.016)
Cu—N1	1.907	1.907	1.907	1.908	1.897	1.905 (1.905)
Cu—N2	1.987	1.982	1.981	1.979	2.009	1.986 (1.986)
Cu'—O1'					2.281	2.321 (2.322)
Cu'—O2'					1.998	2.016 (1.951)
Cu'—O3'					1.943	1.951 (2.016)
Cu'—N1'					1.900	1.905 (1.905)
Cu'—N2'					2.001	1.986 (1.986)
Cu...Cu'					6.78	13.4 (13.4)
N2...N2'					2.76	9.44 (9.44)
Bond angles						
Complex	2	3	4	5	6	7 ^a
O1—Cu—O2	111.5	111.5	111.4	111.5	110.9	111.5 (111.6)
O1—Cu—O3	75.2	75.1	75.1	75.0	76.2	75.4 (75.4)
O2—Cu—O3	162.7	162.6	162.6	162.6	163.8	162.9 (162.9)
O1—Cu—N1	112.2	111.6	111.4	111.3	107.4	112.5 (112.5)
O1—Cu—N2	93.8	94.1	94.1	94.2	102.1	93.8 (93.7)
N1—Cu—N2	152.5	152.8	152.9	153.0	149.0	152.3 (152.4)
O1'—Cu'—O2'					111.7	75.4 (111.5)
O1'—Cu'—O3'					76.7	111.5 (75.4)
O2'—Cu'—O3'					163.6	162.9 (162.9)
O1'—Cu'—N1'					116.0	112.5 (112.5)
O1'—Cu'—N2'					92.6	93.8 (93.7)
N1'—Cu'—N2'					150.0	152.2 (152.4)

^a Metric parameters for isomer *trans* are displayed; the ones for isomer *cis* in parentheses.

Table 4
Selected atomic charges from the NPA analysis for complexes 2–7 as obtained with B3LYP/6-31G(d) ($T = 298$ K).

Complex	2	3	4	5	6	7 ^a
Cu	+1.094	+1.094	+1.094	+1.095	+1.084	+1.092
O1	-0.942	-0.942	-0.942	-0.942	-0.942	-0.942
O2	-0.796	-0.758	-0.759	-0.758	-0.796	-0.760
O3	-0.796	-0.795	-0.795	-0.795	-0.764	-0.796
N1	-0.530	-0.530	-0.530	-0.530	-0.528	-0.530
N2	-0.546	-0.553	-0.550	-0.555	-0.496	-0.543
Cu'					+1.090	+1.092
O1'					-0.943	-0.942
O2'					-0.800	-0.760
O3'					-0.765	-0.796
N1'					-0.526	-0.530
N2'					-0.500	-0.543

^a NPA results for isomers *trans* and *cis* are identical.

the structures of $3 \cdot 2\text{H}_2\text{O}$ and $4 \cdot 2\text{H}_2\text{O}$. While the dipic unit is connected to the apical water molecule *via* two crystallization water molecules in $3 \cdot 2\text{H}_2\text{O}$, the dipic fragment interacts with the monodentate *N*-donor ligand also *via* H-bonds and two crystallization molecules in $4 \cdot 2\text{H}_2\text{O}$. It is worth mentioning that the τ parameter, which helps analyzing the geometry deviation of pentacoordinated environment from the square-pyramidal arrangement ($\tau = 0$) or from the trigonal bipyramidal geometry ($\tau = 1$) [54] shows values of 0.14, 0.15, and 0.20 for $3 \cdot \text{H}_2\text{O}$, $4 \cdot 2\text{H}_2\text{O}$, and $5 \cdot \text{H}_2\text{O}$, respectively. These values are in line with the aforementioned discussed square-pyramidal coordination geometry in all structurally characterized complexes.

3.2. Geometry Optimization, Electronic Structure and NPA Results

Theoretical calculations were conducted for complexes 2–7. It is worth mentioning that the crystallographic data for the dinuclear complex 6 exhibit apically coordinated water molecules *trans* to each other [40,47], while the structural information in 7 accounts for complexes interacting to each other with coordinated water in *cis* orientation [40]. This observation prompted us to optimize the geometry of 7 in a *cis* and a *trans* disposition of their coordinated water (Fig. 4).

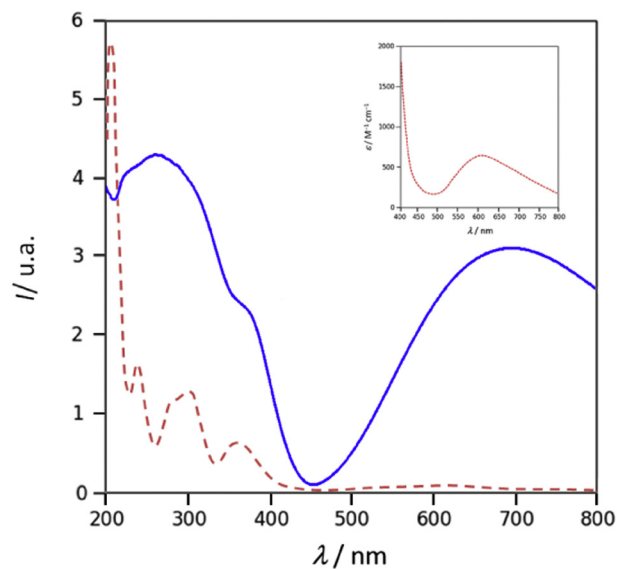


Fig. 5. Experimental UV–VIS reflectance spectrum of 6 measured in the solid state (solid line), and calculated in the gas phase with B3LYP/6-31G(d) (dashed line; inset: calculated spectrum in the VIS region).

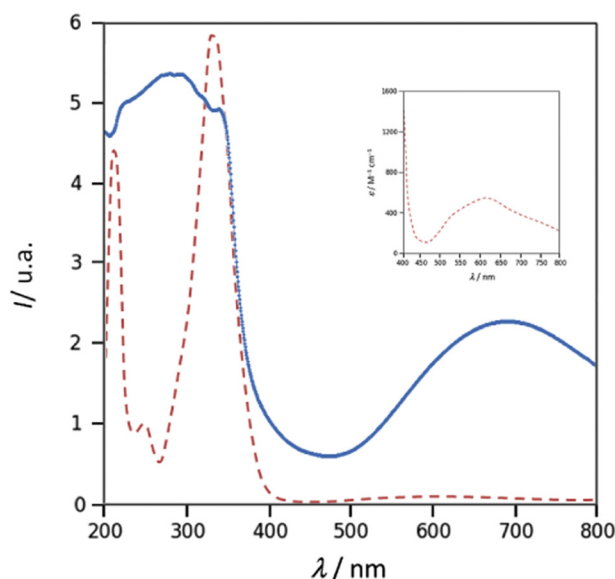


Fig. 6. Experimental UV–VIS spectrum of **7** measured in the solid state (solid line), and calculated for *trans*-**7** in the gas phase with B3LYP/6-31G(d) (dashed line; inset: calculated spectrum in the VIS region).

Geometry optimization led to a minimum as stationary point in all cases (Tables S1–S7). All optimized structures display the metal residing in a slight distorted square-pyramidal environment. Selected optimized parametric are collected in Table 3. The calculated geometries in the gas phase reasonable match the experimental evidence [40,46,47] considering the absence of packing-forces and H-bond effects in the calculations. It is worth mentioning that no systematic improvement of the geometric data has been obtained by employing more extended basis sets (cc-pVDZ and cc-pVTZ; for further details, see Supplementary Information in Table S8).

For dinuclear species, the presence of pyz as bridging-ligand promotes slight modification in the coordination sphere with respect to mononuclear complexes. In case of pypy as bipyridyl-bridge, the selected geometric parameters resemble those calculated for mononuclear compounds. It should be noted that these results are practically not affected by the disposition of the coordinated water molecules, even

when some conformational changes were detected (Cu'—O2' and Cu'—O3' bond lengths, O1'—Cu'—O2' and O1'—Cu'—O3' angles).

Calculated NPA charges on selected atoms are collected in Table 4. The NPA result for copper is smaller than the formal value of +2 as a result of the electron-density donation process. The metal ion ends with a charge of about +1.09, while the non-metal atoms support a charge ranging from −0.528 to −0.942. In all cases, the oxygen apically coordinated delivers a charge density in minor extension than the one of the dipic anion. Nitrogen atoms of the pyridyl ligand and the dipic fragment exhibit similar values of the charge density. The NPA results for the {Cu(dipic)(OH₂)} units in **6** and **7** seems to be not affected by the presence of the *N,N*-bipyridyl connector.

3.3. Electronic Spectra

Complexes **2–6** were characterized by UV–VIS measurements in solution (MeOH) and in the solid state (reflectance measurements), complex **7** being included only in the last studies due to solubility problems in common solvents. TD-DFT calculations led to results in the presence of the solvent with no significant shifts in comparison to those in the gas phase.

In solution, a well-defined band was experimentally observed in the visible region at about 730 nm, which seems to show no dependence on the nature of the substituent on the pyridyl-ring. The UV-portion of the spectrum exhibited an intense and complex band at about 280 nm. In going from the solution to the solid state, remarkable changes were detected. For mononuclear complexes, the nature of the substituent affects the position of the band at the low-energy region. The change in the pyridyl-based ligand from py to pypH led to a systematic hypsochromic shift (of up to −45 nm) (for further details, see Fig. S1). At the same time, the band at the visible emerged as very intense, which is indeed comparable to the one detected in the UV-region. In case of dinuclear complexes, the position of the visible band is not affected by an increase in the length of the connecting ligand (pyz and pypy). It is worth mentioning that the intensity of this band for dinuclear species resulted comparable to the one at the high-part of the spectrum, this observation being in agreement with the results for mononuclear species.

TD-DFT calculations were conducted for species **6** and **7**, the last one being studied in the gas phase in a *cis* and a *trans* orientation of the apically coordinate water molecules (Fig. 4). The TD-B3LYP/6-31G(d) data for **6** and for *trans*-**7** reasonably reproduced the experimental evidence in the solid state (Figs. 5 and 6). In the range 400–800 nm, one well-defined and asymmetric absorption band was detected, for which a blue-shift of up to −80 nm with respect to the experimental information (complex **6**) was calculated. Unlike the one calculated for the *trans* isomer, the simulation for *cis*-**7** accounted for the presence of two bands (Fig. S2). It is worth mentioning that the calculations for all dinuclear complexes were not able to reproduce the relative intensity of the band in the visible portion of the spectrum experimentally observed in the solid state.

By examining the high-energy part of the spectrum, interesting features emerged. For complex **6**, three simulated bands (comparable in intensity) originate the experimental one observed in the UV-region. The results for complex **7**, for which no influence on the disposition of the coordinated water molecules was detected, show a very intense and asymmetric band peaked at about 330 nm, and a second one — significantly less intense — located at about 240 nm. The nature of the bridging ligand promotes differences in charge delocalization of the MOs involved in the UV-region excitations. This finding promotes the aforementioned differences in intensity ratio in the high-energy portion of the spectrum for complexes **6** and **7** (further details are discussed in text below).

The analysis of MOs is very important to get deeper insight into the origin of absorption bands. In Tables 5 and 6, the most important orbital excitations associated with the band experimentally located at 672 and 675 nm for **6** and *trans*-**7**, respectively, are summed up (data for *cis*-**7**

Table 5
Selected orbital excitations calculated for **6** in the gas phase employing TD-B3LYP in combination with 6-31G(d).

Most important excitations ^{a,b}	<i>f</i>	λ_{calc} (nm)	λ_{exp} (nm) ^c	Origin ^d
H − 25(β) → L + 1(β), H − 9(β) → L + 1(β)	0.0023	594.9	672 (720)	MLMLCT
H − 23(β) → L + 2(β), H − 7(β) → L + 2(β)	0.0024	591.2		
H − 12(β) → L(β), H − 10(β) → L(β)	0.0434	358.5	365 (313)	MLLCT
H − 16(α) → L(α)	0.1202	307.1	260 (253, 260, 267,	LLCT
H − 9(β) → L + 3(β)	0.0196	275.3	277)	
H − 7(β) → L + 5(β)	0.0167	273.2		
H − 17(β) → L(β)	0.0106	271.1		
H − 15(β) → L + 6(β)	0.0320	242.7	220 (224)	LLCT
H − 12(β) → L + 6(β)	0.0320	239.5		
H − 27(α) → L(α)	0.2048	211.7	Not detected	
H − 15(α) → L + 3(α)	0.1634	204.4		
H − 15(α) → L + 3(α), H − 1(α) → L + 8(α)	0.1829	203.6		

^a Only those excitations with contribution larger than 15% were considered.

^b H = HOMO; L = LUMO.

^c λ_{exp} (nm) measured in the solid state; the value obtained in solution in parentheses.

^d See in text for acronyms employed in assigning origin of absorption bands.

Table 6
Selected orbital excitations calculated for *trans*-7 in the gas phase employing TD-B3LYP in combination with 6-31G(d).

Most important excitations ^{a,b}	<i>f</i>	λ_{calc} (nm)	λ_{exp} (nm) ^c	Origin ^d
H – 11(β) → L + 1(β)	0.0019	748.8	675	MLMLCT
H – 16(β) → L + 2(β), H – 15(β) → L + 1(β)	0.0016	634.7		
H – 1(α) → L(α), H(α) → L(α)	0.0038	525.5		
H – 12(β) → L(β), H – 10(β) → L(β)	0.3060	347.4	340	MLLCT
H – 10(α) → L(α), H – 12(β) → L(β)	0.6251	326.0		
H – 16(α) → L(α), H – 16(β) → L(β)	0.1153	302.7	272, 291, 318, 220	LLCT
H – 10(α) → L + 1(α)	0.0312	249.8		
H – 16(α) → L + 4(α), H – 15(α) → L + 3(α)	0.0381	212.0 ^e	Not detected	

^a Only excitations with contribution larger than 15% were considered.

^b H = HOMO; L = LUMO.

^c λ_{exp} (nm) observed in the solid state.

^d See in text for acronyms employed in assigning origin of absorption bands.

^e Band originated in many (very) intense excitations, which are associated with weight lower than 4%. The excitations included in table are the only one with contribution larger than 15%.

are included in Supplementary Material, Table S9). In the first case, the charge moves from HOMO – 25(β), HOMO – 23(β), HOMO – 9(β), and HOMO – 7(β) to the LUMO + 1(β) and LUMO + 2(β). Their contours (Fig. 7) allow us assigning the origin of the band at 672 nm for **6** as metal-ligand-to-metal-ligand-charge-transfer (MLMLCT). In analogy to the foregoing results for **6**, the origin of the band at 675 nm for *trans*-7 can be attributed mainly to a MLMLCT, even when a contribution of metal-ligand-to-ligand-charge-transfer (MLLCT) is also observed (Fig. 8).

The band at 365 nm for **6** has its origin in excitations from the HOMO – 12(β) and from the HOMO – 10(β), to the LUMO(β). For complex *trans*-7, orbitals other than the already mentioned are involved in the origin of the band at 340 nm. Indeed, a contribution from the excitation HOMO(α) → LUMO(α) was calculated. While the destination orbitals are mostly bridging-ligand in character in both complexes, the starting orbitals show differences (Fig. 9). For *trans*-7, the connecting-ligand prompts a charge delocalization along its structure in all HOMO-derivatives, which is not displayed in the same extension when pyz acts as bridging-unit in **6**. These findings are in line with a MLLCT assignment for the band at 356 nm for **6** and at 340 for *trans*-7, in the last specie the contribution from a ligand-to-ligand-charge-transfer (LLCT) being of significance. This observation supports also the difference in intensity previously discussed.

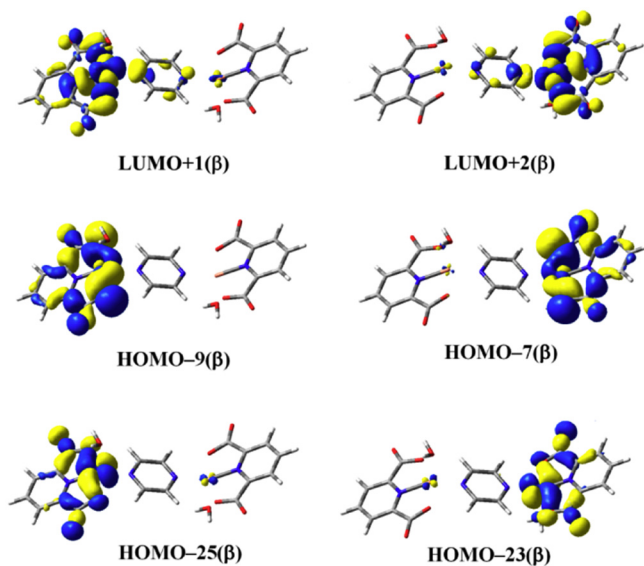


Fig. 7. HOMO- and LUMO-derivatives of **6** as calculated with B3LYP/6-31G(d) involved in the origin of the absorption band in the visible region of the spectrum (isoelectronic cut-off of 0.25 e A^{-3}).

The contours of the HOMOs and LUMOs implicated in the detected band under 300 nm enable assuming mainly a LLCT as its origin (for further details, see Supplementary Information, Figs. S3 and S4).

It is well-known that B3LYP is usually unsuccessful in dealing with long-range charge-transfer processes. Even when it is our intention to use TD-DFT as a complement of the experimental evidence in this contribution, an assessment of the performance of B3LYP mainly at the blue-part of the spectrum for title complexes was conducted. In this line, CAM-B3LYP [55] was chosen and therefore, TD-DFT/CAM-B3LYP/6-31G(d) calculations in the gas phase and in the presence of MeOH as solvent (C-PCM) were performed for all dinuclear complexes. As with B3LYP, non-important shifts were detected in going from the gas phase to the solution. The simulation led to analogous results to B3LYP in the VISIBLE region; in the UV, differences worth to be highlighted were observed mainly for complex **6** (further details in Supplementary Information). In this case, four bands were detected. In contrast to B3LYP, CAM-B3LYP led to a very weak band at 359 nm, while a very intense band was simulated at 234 nm. The MOs involved in the excitation point to a LLCT as origin of the bands experimentally found in the blue-part of the spectrum. Thus, CAM-B3LYP removed the “metal-ligand” character obtained with B3LYP in the starting MOs involved in all important excitations. When the situation of complex **7** is analyzed, the

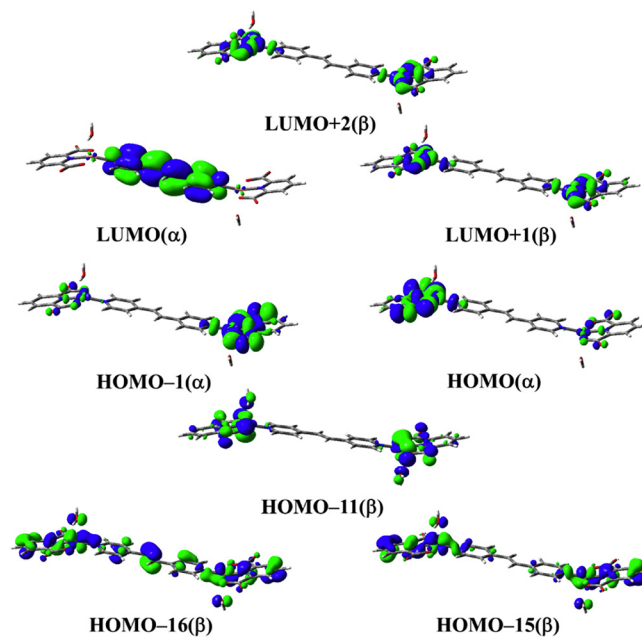


Fig. 8. HOMO- and LUMO-derivatives of *trans*-7 as calculated with B3LYP/6-31G(d) involved in the origin of the absorption band in the visible region of the spectrum (isoelectronic cut-off of 0.25 e A^{-3}).

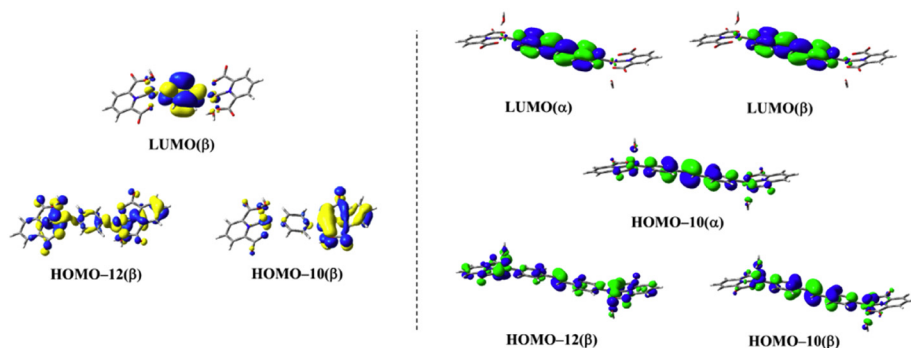


Fig. 9. HOMO- and LUMO-derivatives of **6** (left) and *trans*-**7** (right) – responsible for the band at about 350 nm – calculated with B3LYP/6-31G(d) (isoelectronic cut-off of $0.25 \text{ e} \text{ \AA}^{-3}$).

trans disposition is taken as example. In this case, a blue-shift of the band-pattern observed in the UV-region with B3LYP was obtained with CAM-B3LYP. A very intense band – product of a single excitation ($f = 1.4512$) – was simulated at 284.1 nm, which represents about –60 nm of displacement with respect to B3LYP. The analysis of MOs conducts again to a LLCT as origin of the absorption bands in the UV.

In our opinion, B3LYP proved to be successfully enough to complement the experimental evidence in studying absorptive features of dinuclear Cu(II) complexes with dipicolinate and pyridyl-based.

4. Concluding Remarks

Three new complexes of Cu(II) with dipicolinate and pyridyl-based ligands were afforded by a simple substitution reaction starting from the precursor *mer*-[Cu(dipic)(OH)₂]₃, and were structurally characterized. The crystallographic data accounted for slight distorted square-pyramidal structures in which dipicolinate coordinates the metal center in a *mer*-fashion. A water molecule was detected apically coordinated and the pyridyl ligand completes the coordination sphere. A mononuclear complexes and two dinuclear complexes, for which only X-ray structures were reported, were also prepared and characterized in this contribution to study the effect of the pyridyl-substituent on properties in solution and on absorptive features in the UV–VIS region (in solution and in the solid state).

The structure and electronic properties of all complexes were studied by DFT methods at the B3LYP/6-31G(d) level of theory. This methodology reasonably reproduced metric data at a very low computational cost. The absorptive features of dinuclear complexes, which bear *N,N'*-dipyridyl-bridge with different conjugation extension, were explored by TD-DFT/B3LYP/6-31G(d) calculations. This method proved to be suitable in reproducing the electronic UV–VIS absorption spectra, and allowed us to explain the origin of the absorption bands experimentally detected.

Crystallographic data for the structural analysis have been deposited with the Cambridge Crystallographic Data Centre (CCDC) reference numbers 1425657 (Cu-dipic-pic), 1441008 (Cu-dipic-pyph), and 1501745 (Cu-dipic-vpy). A copy of this information may be obtained via <http://www.ccdc.cam.ac.uk>, or from the Cambridge Crystallographic Data Centre, 12 Union Road, Cambridge CB2 1EZ, UK; fax: (+44) 1223-336-033, or e-mail: deposit@ccdc.cam.ac.uk. Supplementary data associated with this article can be found in the online version, at <http://dx.doi.org/10.1016/j.saa.2017.04.003>.

Acknowledgements

This work was partially supported by CSIC (Programa de Apoyo a Grupos de Investigación). F. Luzardo is indebted to Agencia Nacional de Investigación e Innovación (ANII, Uruguay) for a scholarship. A. S. S. de Camargo acknowledge the financial support of FAPESP – Fundação de Amparo a Pesquisa do Estado de São Paulo through CEPID grant 2013/07793-6.

References

- [1] R. Lukes, M. Jurecek, Collect. Czech. Chem. Commun. 13 (1948) 131.
- [2] R.L. Dutta, S. Ghosh, J. Indian Chem. Soc. 44 (1967) 273.
- [3] M.G.B. Drew, R.W. Matthews, R.A. Walton, J. Chem. Soc. A (1970) 1405.
- [4] D.P. Murtha, R.A. Walton, Inorg. Chem. 12 (1973) 1278.
- [5] H. Gaw, W.R. Robinson, R.W. Walton, Inorg. Nucl. Chem. Lett. 7 (1971) 695.
- [6] M.B. Cingi, A.C. Villa, C. Guastini, M. Nardelli, Gazz. Chim. Ital. 101 (1971) 825.
- [7] B. Zhao, P. Cheng, Y. Dai, C. Cheng, D.Z. Liao, S.P. Yan, Z.H. Jiang, Angew. Chem. Int. Ed. 42 (2003) 934; Angew. Chem. 115 (2003) 964.
- [8] D. Deng, P. Liu, W. Fu, L. Li, F. Yang, B. Ji, Inorg. Chim. Acta 363 (2010) 891.
- [9] M.L. Tong, J. Wang, S. Hu, J. Solid State Chem. 178 (2005) 1518.
- [10] B. Zhao, H.L. Guo, X.L. Cheng, P. Cheng, W. Shi, D.Z. Liao, S.P. Yan, Z.H. Jiang, Chem. Eur. J. 12 (2006) 149.
- [11] H.L. Guo, B. Ding, L. Yi, P. Cheng, D.Z. Liao, S.P. Yan, Z.H. Jiang, Inorg. Chem. Commun. 8 (2005) 151.
- [12] J.C. MacDonald, T.J.M. Luo, G.T.R. Palmore, Cryst. Growth Des. 4 (2004) 1203.
- [13] S.X. Cui, Y.L. Zhao, J.P. Zhang, Q. Liu, Y. Zhang, Cryst. Growth Des. 8 (2008) 3803.
- [14] M.S. Liu, Q.Y. Yu, Y.P. Cai, C.Y. Su, X.M. Lin, X.X. Zhou, J.W. Cai, Cryst. Growth Des. 8 (2008) 4083.
- [15] L.L. Wen, Y.Z. Li, Z.D. Lu, J.G. Lin, C.Y. Duan, Q.J. Meng, Cryst. Growth Des. 6 (2006) 530.
- [16] B.O. Patrick, C.L. Stevens, A. Storr, R.C. Thompson, Polyhedron 22 (2003) 3025.
- [17] A.M. Beatty, B.A. Helfrich, G.A. Hogan, B.A. Reed, Cryst. Growth Des. 6 (2006) 122.
- [18] J.C. MacDonald, P.C. Dorrestein, M.M. Pilley, M.M. Foote, J.L. Lundburg, R.W. Henning, A.J. Schultz, J.L. Manson, J. Am. Chem. Soc. 122 (2000) 11692.
- [19] S.K. Ghosh, J. Ribas, P.K. Bharadwaj, CrystEngComm 6 (2004) 250.
- [20] L. Yang, D.C. Crans, S.M. Miller, A. Cour, O.P. Anderson, P.M. Kaszynski, M.E. Godzala, L.-T.D. Austin, G.R. Willsky, Inorg. Chem. 41 (2002) 4859.
- [21] R. Hernandez-Molina, V.P. Fedin, M.N. Sokolov, D.M. Sellsell, A.G. Sykes, Inorg. Chem. 37 (1998) 4328.
- [22] D.M. Sellsell, A.G. Sykes, Inorg. Chem. 35 (1996) 5536.
- [23] C.G. Sellsell, C.D. Borman, A.J. Baron, M.J. McPherson, A.G. Sykes, Inorg. Chem. 36 (1997) 4520.
- [24] A.G. Mauk, C.L. Coyle, E. Bordignon, H.B. Gray, J. Am. Chem. Soc. 101 (1979) 5054.
- [25] A.G. Mauk, C.L. Coyle, E. Bordignon, B. Gray, J. Am. Chem. Soc. 104 (1982) 7654.
- [26] L.C. Nathan, D.C. Zapfen, A.M. Mooring, C.A. Doyle, J.A. Brown, Polyhedron 8 (1989) 745.
- [27] D.L. Hoof, R.A. Walton, Inorg. Chim. Acta 12 (1975) 71.
- [28] R.W. Matthews, A.D. Hamer, D.L. Hoof, D.G. Tisley, R.A. Walton, J. Chem. Soc. Dalton Trans. 1035 (1973).
- [29] J.F. Powell, Biochemistry 54 (1953) 205.
- [30] B.S. Church, H. Halvorson, Nature 183 (1959) 124.
- [31] L. Chung, K.S. Rajan, E. Merdinger, N. Crez, Biophys. J. 11 (1971) 469.
- [32] N. Okabe, N. Oya, Acta Cryst C56 (2000) 1416.
- [33] B.L. Martin, Arch. Biochem. Biophys. 345 (1997) 332.
- [34] Y. Pocker, C.T.O. Fong, Biochemistry 19 (1980) 2045.
- [35] G. Scapin, S.G. Reddy, R. Zheng, J.S. Blanchard, Biochemistry 36 (1997) 15081.
- [36] W.L.F. Armarego, D.D. Perrin, Purification of Laboratory Chemicals, fourth ed. Butterworth-Heinemann, Woburn, 2000.
- [37] L. Kürti, B. Czako, Knoevenagel Condensation in: Strategic Applications of Named Reactions in Organic Synthesis, first ed. Elsevier Inc., India, 2012 242.
- [38] Procedure for Knoevenagel condensation reaction for ligand *pyph*: 400 μL (4.12 mmol) of 4-picoline were deprotonated with 3.0 mL (4.32 mmol) of lithium diisopropylamide (LDA) in 5 mL dry tetrahydrofuran (THF) at -70°C . Thereafter and in the absence of light, 500 mL (4.32 mmol) of benzaldehyde was slowly added, the reaction mixture being stirred at reflux conditions in the presence of 10 mL of acetic acid during 24 h. After purification by column chromatography (silica gel; hexane:ethyl acetate, 7:3, v/v), a pale-yellow solid was obtained (473 mg, 63%). ^1H RMN (400 MHz, CDCl_3 , δ): 8.60 (d, $J = 8$ Hz, 2H, Ar-H), 7.56 (d, $J = 8$ Hz, 2H, Ar-H), 7.42 (d, $J = 8$ Hz, 2H, Ar-H), 7.38 (d, $J = 8$ Hz, 3H, Ar-H, Ar-H), 7.32 (d, $J = 16$ Hz, 1H, $-\text{CH}=\text{CH}-$), 7.03 (d, $J = 16$ Hz, 1H, $-\text{CH}=\text{CH}-$). Ligand *pyph*: 400 μL (4.12 mmol) of 4-picoline reacted with 3.0 mL (4.32 mmol) of LDA in THF (5 mL) at -70°C . In the absence of light, 465 mL (4.12 mmol) of 4-pyridinylcarboxaldehyde was dropwise added with continuous stirring. After 24 h of reflux in the presence of 10 mL of acetic acid, the reaction mixture led to a yellow

- solution, from which a pale-yellow solid was separated by rotatory evaporation. The solid was purified employing column chromatography in analogous conditions to the ones previously mentioned (368 mg, 49%). ¹H RMN (400 MHz, CDCl₃, δ): 8.62 (d, *J* = 4 Hz, 4H, Ar–H), 7.61 (d, *J* = 4 Hz, 4H, Ar–H), 7.55 (s, 2H, –CH=CH–).
- [39] P.K. Bhowmik, A.K. Nedeltchev, H. Han, *Tetrahedron Lett.* 48 (2007) 5383.
- [40] M. Felloni, A.J. Blake, P. Hunnerstey, C. Wilson, M. Schröder, *Cryst. Growth Des.* 9 (2009) 4685.
- [41] Bruker, APEX2 (Version 2008.1-0), Bruker AXS Inc., Madison, Wisconsin, USA, 2008.
- [42] R. Blessing, *Acta Crystallogr. Sect. A* 51 (1995) 33.
- [43] G.M. Sheldrick, *Acta Crystallogr. Sect. A* 64 (2008) 112.
- [44] C.B. Hubschle, G.M. Sheldrick, B. Dittrich, *J. Appl. Cryst.* 44 (2011) 1281.
- [45] L.J. Farrugia, *J. Appl. Cryst.* 45 (2012) 849.
- [46] B. Das, J.B. Baruah, *Polyhedron* 31 (2012) 361.
- [47] (a) A.D. Becke, *Phys. Rev. A* 38 (1988) 3098;
(b) A.D. Becke, *J. Chem. Phys.* 98 (1993) 1372;
(c) C. Lee, W. Yang, R.G. Parr, *Phys. Rev. B* 37 (1988) 785.
- [48] P.C. Hariharan, J.A. Pople, *Theor. Chim. Acta* 28 (1973) 213;
- (b) M.M. Francl, W.J. Pietro, W.J. Hehre, J.S. Binkley, M.S. Gordon, D.J. DeFrees, J.A. Pople, *J. Chem. Phys.* 77 (1982) 3654;
- (c) V. Rassolov, J.A. Pople, M. Ratner, T.L. Windus, *J. Chem. Phys.* 109 (1998) 1223.
- [49] (a) V. Barone, M. Cossi, *J. Phys. Chem. A* 102 (1998) 1995;
(b) M. Cossi, N. Rega, G. Scalmani, V. Barone, *J. Comput. Chem.* 24 (2003) 669.
- [50] N.M. O'Boyle, A.L. Tenderholt, K.M. Langner, *J. Comput. Chem.* 29 (2008) 839.
- [51] (a) J.P. Foster, F. Weinhold, *J. Am. Chem. Soc.* 102 (1980) 7211;
(b) A.E. Reed, F. Weinhold, *J. Chem. Phys.* 83 (1985) 1736;
(c) A.E. Reed, R.B. Weinstock, B. Weinhold, *J. Chem. Phys.* 83 (1985) 735;
(d) A.E. Reed, L.A. Curtis, F. Weinhold, *Chem. Rev.* 88 (1988) 899.
- [52] M.J. Frisch, et al., GAUSSIAN 09, Rev. D01, Gaussian, Inc., Wallingford, CT, 2009.
- [53] A.W. Addison, T.N. Rao, J. Reedijk, J.V. Rijn, G.C. Verschoor, *J. Chem. Soc. Dalton Trans.* (1984) 1349.
- [54] E. Altin, R. Kirchmaier, A. Lentz, *Z. Kristallogr. - New Cryst. Struct.* 219 (2004) 137.
- [55] T. Yanai, D.P. Tew, N.C. Handy, *Chem. Phys. Lett.* 393 (2004) 51.